Environmental Science & Technology

pubs.acs.org/est

Article

Photodegradation Processes and Weathering Products of Microfibers in Aquatic Environments

Shimaa M. Kteeba and Laodong Guo*

Cite This: *Environ. Sci. Technol.* 2024, 58, 16535−16546

Read Online

ACCESS | Metrics & More | Article Recommendations | Supporting Information

ABSTRACT: Microplastics, particularly microfibers (MFs), pose a significant threat to the environment. Despite their widespread presence, the photochemical reactivity, weathering products, and environmental fate of MFs remain poorly understood. To address this knowledge gap, photodegradation experiments were conducted on three prevalent MFs: polyester (POL), nylon (NYL), and acrylic (ACR), to elucidate their degradation pathways, changes in surface morphology and polymer structure, and chemical and colloidal characterization of weathering products during photochemical degradation of MFs. The results showed that concentrations of dissolved organic carbon, chromophoric dissolved organic matter (DOM), and fluorescent components consistently increased during weathering, exhibiting a continuous release of DOM. Scanning electron microscopy and Raman spectroscopy revealed changes in the surface morphology and polymer spectra of the MFs. During the weathering experiments, DOM aromaticity ($SUVA_{254}$) decreased, while spectral slope increased, indicating concurrent DOM release and degradation of aromatic components. The released DOM or nanoplastics were negatively charged with sizes between 128 and 374 nm. The production rate constants of DOM or the photochemical reactivity of MFs followed the order ACR > NYL ≥ POL, consistent with their differences in chemical structures. These findings provide an improved understanding of the photochemical reactivity, degradation pathways, weathering products, and environmental fate of microfibers in the environment.

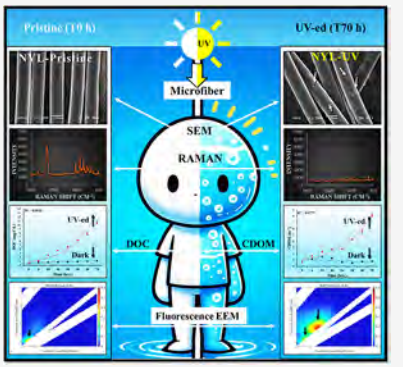

KEYWORDS: *microfibers, microplastics, nanoplastics, dissolved organic matter, photochemical degradation, surface properties, environmental fate*

1. INTRODUCTION

Microplastic pollution in aquatic environments has become an escalating environmental concern.[1,2] A substantial proportion of plastics are discarded after use, and only 6−26% are recycled before being disposed of, reflecting the challenges posed by mass production and inadequate plastic management in recent decades.[3,4] In addition to environmental impacts from plastic debris, the fragmentation and degradation of plastic debris and microplastics have been shown to release dissolved organic matter (DOM) in aquatic environments.[5−7] As microplastics undergo photodegradation, the polymer chains break down into smaller fragments, resulting in the formation of small plastic particles with dimensions varying from micro- to nanoscales.[9,10,12] These newly formed nanomaterials may exhibit distinct properties and behaviors compared to their larger counterparts, influencing their interactions with ecosystems, organisms, and potentially posing novel challenges in environmental and biogeochemical processes in aquatic environments.[5,13,14] However, specific pathways and mechanisms of microplastic degradation and DOM production remain poorly understood.

Beyond pollution from microplastics and plastic debris, microfibers, primarily composed of synthetic polymers, could account for over 90% of the total amount of microplastics found in aquatic environments.[8,15] Indeed, microfibers have been reported as being widespread in not only environmental samples but also drinking waters and biota.[16,17] In addition to synthetic microfibers, cellulosic and cotton fibers are dominant microfiber pollution in various environmental compartments.[18−20] Synthetic fibers, like polyester, nylon, and acrylic, are often used in clothing, carpets, and other textiles and can shed into the environment during use and laundering. Therefore, one major contributor to microfiber pollution arises from the washing of textiles and synthetic materials,[15] and the discharge of synthetic fibers into the environment include atmospheric deposition[21,22] and sewage effluent, with polyester and acrylic making up the majority.[23] These microfibers can ultimately end up in rivers, lakes, oceans, and other aquatic systems.[8,18,24−26,28,29]

The presence of microfibers has detrimental effects on marine life and aquatic organisms.[27,30−32] Due to their static

Received: April 17, 2024
Revised: August 24, 2024
Accepted: August 26, 2024
Published: August 31, 2024

https://doi.org/10.1021/acs.est.4c03667
Environ. Sci. Technol. 2024, 58, 16535−16546

electric charge and available surface areas, microfibers can absorb hazardous chemicals, heavy metals, and oil that already exist in the water.[33,34] Moreover, microfibers exhibit a more significant leaching of water-soluble DOM with high resistance to photochemical degradation compared to other microplastics.[35,36] Despite the significance of MFs in the environment, their photochemical reactivity, degradation products, and environmental fate in aquatic systems are largely unknown. Much previous research focused mostly on the occurrence and degradation of other microplastics.[6,9,37−40] Studies on the photochemical degradation and resultant weathering products of MFs remain scarce.[8,41] To fill the knowledge gap, three prevalent microfibers, including polyester (POL), nylon (NYL), and acrylic (ACR), were utilized in our degradation experiments to investigate the photochemical degradation processes and weathering products of MFs.

Our major objectives were to (1) elucidate the relative photochemical reactivity of different microfibers (MFs) and the release of DOM under ultraviolet (UV) irradiance, (2) assess changes in surface morphology and polymeric structure of microfibers during photochemical weathering, and (3) characterize the optical, chemical, and colloidal properties of DOM released from MFs and their variations during the photochemical degradation of MFs. We found that UV irradiation significantly altered the surface morphology and polymeric spectra of all microfibers, leading to a continuous release of nanosized DOM following a linear or exponential trend. New results from this study provide insights into the photodegradation pathways, weathering products, and environmental fate of MFs in aquatic environments.

2. MATERIALS AND METHODS

2.1. Microfibers Used and Pretreatments. Three of the most common MFs were selected for degradation experiments to evaluate their degradation behavior and the production of DOM during photochemical weathering. They are polyester (POL) having a thickness of 2.0 denier (D) and 3.2 mm in length, nylon 66 (NYL) with 1.0 D and 3.2 mm length, and acrylic (ACR) with 15.0 D and 0.05 mm length (Table 1).

Table 1. List of Microfibers and Their Physical Properties, Chemical Formula, and Monomer Structure

Fiber	ID	Denier (or diameter in μm)	Length (mm)	Chemical formula	Monomer structure	Molar mass (g/mol)
Polyester	POL	2.0 (17.8)	3.2	$(C_{10}H_8O_4)_n$		228.20
Nylon 66	NYL	1.0 (12.2)	3.2	$(C_{12}H_{22}N_2O_2)_n$		226.32
Acrylic	ACR	15.0 (48.6)	0.05	$(-CH_2-CH(CN)-)_n$		53.06

These pristine minifibers (dye-free and additive-free) were obtained from Testfabrics, Inc. (West Pittston, PA, U.S.A.). All MFs were prewashed 3 times with ultrapure water by sonicating the suspension and filtration to remove water-soluble DOM before UV exposure.

2.2. Photochemical Degradation of MFs. Prewashed MFs were dispersed in ultrapure water (with a weight/volume ratio of 1 g/200 mL) in pre-combusted glass beakers with quartz lids. Replicate samples were kept in the dark to serve as controls for the light experiments. Degradation experiments were conducted under a 400 W UV lamp (MH1-400EB), with an irradiance of 850 W m^{-2} for a total of 70 h. Time series samples were collected at 0, 4, 6, 12, 24, 48, and 70 h from both light and dark treatments for the characterization of DOM released from MFs. Evaporation during UV irradiation was compensated by adding ultrapure water before each sampling.[36] All time-series samples were consistently filtered through pre-combusted GF/F filters (Whatman) to remove any possible particles.

2.3. Morphological Characterization of MFs Using Scanning Electron Microscopy (SEM). SEM (JEOL JSM6460-LV) was utilized to examine the changes in the surface morphology of pristine MFs before and after degradation. Gold/palladium (Au/Pd), a metal with excellent electrical conductivity, was coated/sputtered onto MFs (a non-conducting specimen) using the Denton Vacuum Desk II sputter coater, with a coating thickness of 6−8 nm. Images were taken at various magnifications with a working distance of 12 mm and an accelerating voltage ranging between 8 and 10 kV.

2.4. Polymer Structure of MFs by Raman Spectroscopy. A Raman spectrometer (model 1000B,Renishaw) equipped with an Olympus (Melville, NY, U.S.A.) BHSM metallurgical microscope was used for the collection of Raman spectra. A 785 nm, 300 mW, continuous wave, wavelength-stabilized laser diode (SDL, San Jose, CA, U.S.A.) was selected as the excitation source. A 20× microscope objective was utilized for all scans. Spectra were collected between 100 and 3600 cm^{-1}. Renishaw Windows-based Raman environment (WIRE) was used for performing spectral acquisition and analysis with 60 s scan time settings.

2.5. Measurements of Dissolved Organic Carbon (DOC). A Shimadzu total organic carbon (TOC) analyzer (TOC-L) with an ASI-L autosampler was used to measure the concentrations of DOC using the high-temperature combustion method.[42] Samples were acidified with HCl to a pH of ≤2 and sparged with air to remove any inorganic carbon. Prior to sample analysis, calibration curves were prepared. In addition, ultrapure water, consensus reference DOC samples (from the University of Miami), and working DOC standards were measured as samples to ensure data quality.[43]

2.6. Ultraviolet−Visible (UV−Vis) Spectroscopic Characterization. Using an Agilent 8453 spectrophotometer and a quartz cuvette with a 1 cm path length, UV−vis absorption spectra were obtained for the wavelength range of 190−1100 nm at 1 nm intervals. Before analyses, ultrapure water was scanned as blanks.[44] The absorption coefficient at 254 nm (a_{245}, m^{-1}) was calculated by multiplying the absorbance with 2.303 and divided by the cuvette path length (in meters). Specific UV absorbance at 254 nm ($SUVA_{254}$, L mg-C^{-1} m^{-1}) was calculated as the ratio of a_{245} to DOC concentration, which provides information on DOM aromaticity.[45] Spectral slope ($S_{275-295}$), which is inversely related to the molecular weight of DOM, was determined by a linear fit of the logarithm of absorption data in the wavelength range of 275−295 nm.[46]

2.7. Fluorescence Excitation−Emission Matrices (EEMs). Fluorescence EEMs were measured using a spectrofluorometer (RF-6000, Shimadzu). Samples in a 1 cm path-length quartz cuvette were scanned at excitation wavelengths ranging from 250 to 480 nm with 5 nm intervals and emission wavelengths ranging from 280 to 600 nm with 2 nm intervals. Ultrapure water was scanned before sample analysis.[43] The scanning speed was 6000 nm/min, and the

https://doi.org/10.1021/acs.est.4c03667
Environ. Sci. Technol. 2024, 58, 16535−16546

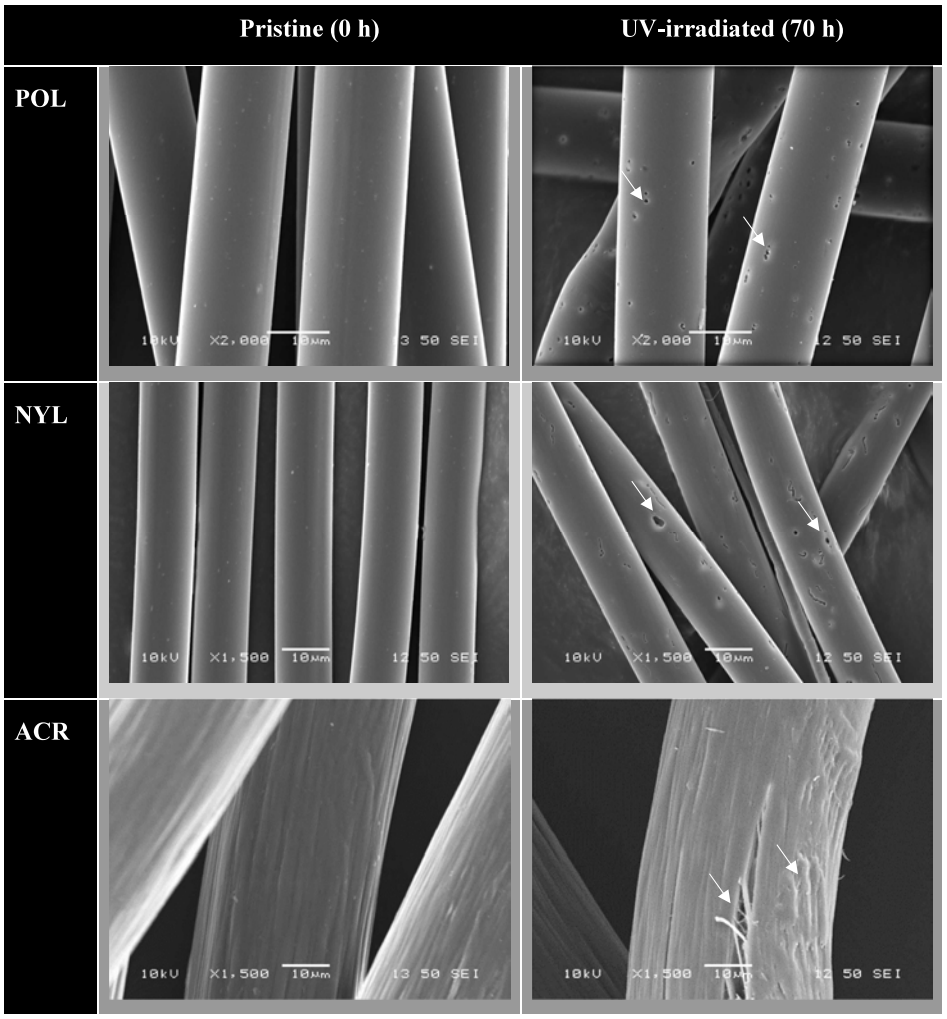

Figure 1. SEM images of pristine (0 h) and weathered (70 h) MFs, including polyester (POL), nylon (NYL), and acrylic (ACR).

excitation and emission bandwidths were set at 5.0 nm with a high instrumental sensitivity. The fluorescence index (FIX), an indicator of the DOM source and freshness, was calculated as the ratio of fluorescence intensities between emission wavelengths of 450 and 500 nm at an excitation wavelength of 370 nm.[48] The humification index (HIX), which provides insight into the degree of DOM humification, was calculated as the ratio of fluorescence signals over the emission range of 435−480 nm to those over the range of 300−345 and 435−480 nm at an excitation wavelength of 254 nm.[49]

2.8. Molecular Size and Zeta Potential. A Zetasizer (Nano ZS, Malvern) was used to measure surface properties, including the zeta potential and molecular size, of DOM released from MFs. The instrument performance was evaluated using standard polystyrene (PS)−latex nanoparticles with a mode size of 100 nm.[50]

2.9. Statistical Analysis. Statistical analyses [e.g., analysis of variance (ANOVA), *t* test, and significance] were performed with Microsoft Excel software (version 2321). A significant level was set at $p < 0.01$.

3. RESULTS AND DISCUSSION

3.1. Changes in Morphological and Structural Properties of Microfibers during Weathering. The surface physical morphology of microfibers was assessed before and after UV irradiation through SEM to examine the relationship between DOM release and changes in the surface morphology of microfibers. As shown in Figure 1, all MFs exhibited evident degradation or morphological alterations on their surfaces following 70 h of UV irradiation. Both POL and NYL demonstrated the formation of holes on their surfaces, although NYL had a higher extent of degradation with numerous irregular inscriptions. In comparison to POL and NYL, ACR exhibited a unique pattern characterized by longitudinal fractures, clearly visible filament fragments, and a roughened surface with embrittled ends.

As shown in Figure 1, the degradation extent among the three MFs followed the sequence ACR > NYL > POL. Notably, both ACR and NYL fibers revealed fragmentation and production of fractal fibers, whereas POL did not exhibit such characteristics. The alterations in microfiber surfaces induced by UV irradiation and the differences in the degradation extent are likely to result in divergent releases of monomers and micro/nanofragments. The fragmentation of MFs tends to be crucial for changing the level of bioavailability, primarily by reducing the particle size and rendering them more accessible to microorganisms.[51] Alterations in surface morphology and the degree of fragmentation may also influence the dispersion of MFs within the water column and their overall environmental fate and behavior.[41]

https://doi.org/10.1021/acs.est.4c03667
Environ. Sci. Technol. 2024, 58, 16535−16546

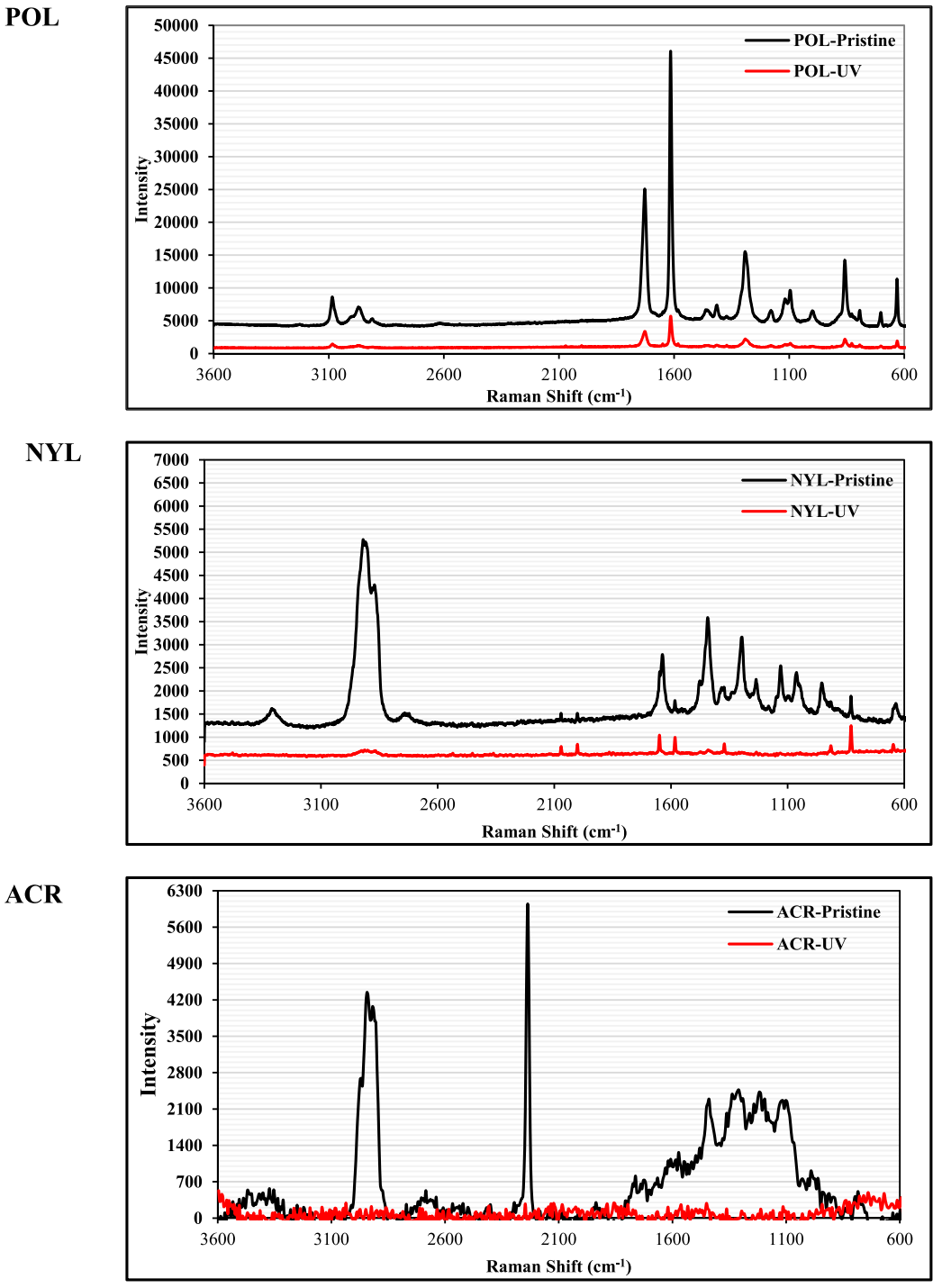

Figure 2. Raman spectra showing changes in surface polymeric spectra of microfibers (POL, NYL, and ACR) before (0 h or pristine) and after (70 h, red colored) UV irradiation.

In addition to alterations in surface morphology, Raman spectroscopy analysis uncovered changes in polymeric spectra of microfiber surfaces with significantly weakened and/or invisible peaks ($p < 0.0001$) observed after UV irradiation (Figure 2). The observed weakening of Raman peaks in weathered microfibers is likely due to increased surface roughness and particle deposition. Nevertheless, the major Raman peaks remained consistent in the weathered microfibers with deviations of 2−3% for polyester, 2% for nylon, and 10% for acrylic in their normalized peaks between pristine and weathered samples (Table S1 of the Supporting Information).

Raman spectroscopy has been used to analyze the vibrational modes of molecules in polymeric materials, including microfibers.[52] Specific Raman peaks for polyester include the aromatic C═C stretching peak at 1615 cm^{-1},[11,53,54] which exhibited an approximately 87% reduction in intensity after photoweathering (Figure 2). Additionally, the polyester structure contains the ester functional group in its backbone, contributing to the C═O stretching vibration observed at ∼1700 cm^{-1} in Raman spectra.[52] As observed in this study, UV irradiation could trigger the breakdown of ester linkages in the polymer backbone.[55] The intensity of the

https://doi.org/10.1021/acs.est.4c03667
Environ. Sci. Technol. 2024, 58, 16535−16546

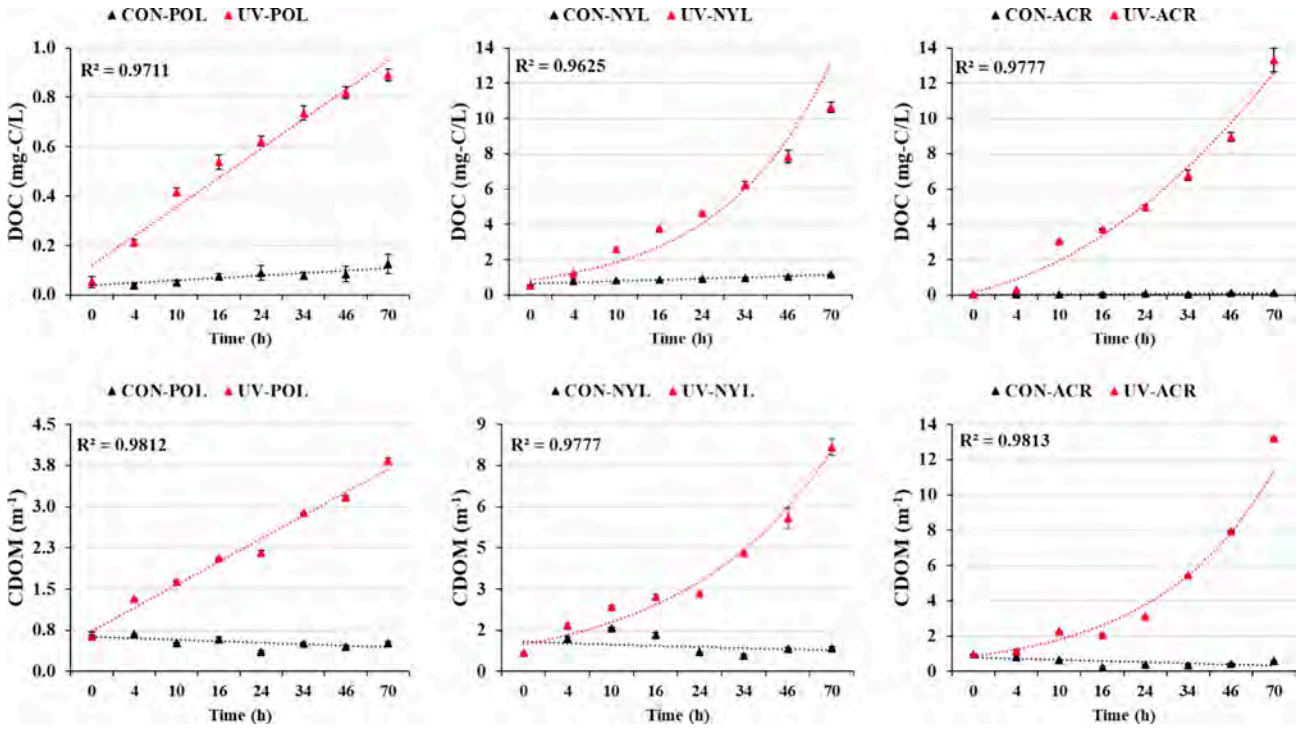

Figure 3. Production of DOC and CDOM (in terms of a_{245}) released from MFs, including POL, NYL, and ACR, during photochemical weathering (UV, red colored) compared to control experiments (CON) under dark incubation.

carbonyl peak at ~1700 cm^{-1} decreased over time, and after 70 h of UV irradiation, a notable 80% reduction in peak intensity is accompanied by peak broadening. Other peaks in the Raman spectrum of polyester include the C−H bending peak at 1450 cm^{-1} and the C−H stretching peak at ~2920 cm^{-1}, indicative of the presence of carbon−hydrogen.[54] These peaks experienced respective intensity losses of 81 and 77% following photoweathering. The evident weakening of bonds and chain scission occurred, leading to a decrease in the strength of POL during degradation.[56]

The Raman spectrum of nylon exhibited several characteristic peaks, including a broad band at 3300 cm^{-1} attributed to N−H stretching vibrations in the amide group.[57] This band experienced a 61% reduction in intensity after weathering (Figure 2). Furthermore, the symmetric stretching vibration of the CH_2 groups in the aliphatic backbone at ~2930 cm^{-1} and the C−H stretching vibration at 2878 cm^{-1} both lost ~85% of their peak intensities. The peak at around 1640 cm^{-1} is associated with the amide I band, which arises from the stretching vibration of the C═O bond in the amide group (−CONH−). Its intensity dropped by 73% after photoweathering. Other peaks in the Raman spectrum of nylon 66 include those associated with aromatic C═C stretching vibrations and C−N stretching vibrations. Various peaks were observed in the pristine MFs but lost 65−78% of their initial intensities after photoweathering, including those at 1489 and 1448 cm^{-1} which are indicative of N−H bending vibration in the amide group and aliphatic chain, respectively. Peaks around 1390 and 1306 cm^{-1}, which are related to the C−H bending vibration in the aliphatic chain, have been detected. Moreover, peaks at 1381 and 1239 cm^{-1} are related to the amide group's C−N stretching vibration. At 1137 cm^{-1}, this peak corresponds to the C−C stretching vibration in the aliphatic chain.[58] The distinctive nitrile band around 2240 cm^{-1} serves as a most prominent spectral feature of acrylics (Figure 2), setting it apart from other microfibers in the Raman spectra.[59,60] The peak at 2963 cm^{-1} arises from CH_3 antisymmetric stretching (methyl group). Although specific details regarding the impact of UV irradiation on the Raman spectra of acrylic are limited, it is evident that UV irradiation has a significant influence on the molecular vibrations, leading to the disappearance of major peaks. This phenomenon serves as a compelling proxy for the degradation of acrylic microfiber and changes in chemical characteristics. Overall, the results revealed by Raman spectroscopy are compatible with the changes observed in surface morphology from SEM (Figure 1) and DOM release during MF weathering, even though the much-weakened Roman spectra of the weathered fibers need further quantification.

3.2. DOM Release during Photochemical Weathering of Microfibers. Variations in the concentrations of DOM, including DOC and chromophoric dissolved organic matter (CDOM) (in terms of a_{245}), released from microfibers during photochemical degradation are depicted in Figure 3. Concentrations of both DOC and CDOM progressively increased with time during photochemical degradation of all three MFs, indicating substantial DOM production from MFs during weathering. However, each MF has a distinctive trendline or pattern in the variation of DOC and CDOM with time (Figure 3). For example, the concentrations of POL-DOM (both DOC and CDOM) increased monotonically or linearly, while those of NYL-DOM and ACR-DOM increased exponentially during photochemical weathering.

These seemingly random variation trends in DOM release during photochemical weathering of different microfibers are intricately linked to their alterations in both surface morphology and Raman spectra (Figures 1 and 2). For example, only minor alteration in polyester surfaces was observed after UV irradiation (Figure 1), and the corresponding DOM release from polyester was linear following a zero-

https://doi.org/10.1021/acs.est.4c03667
Environ. Sci. Technol. 2024, 58, 16535−16546

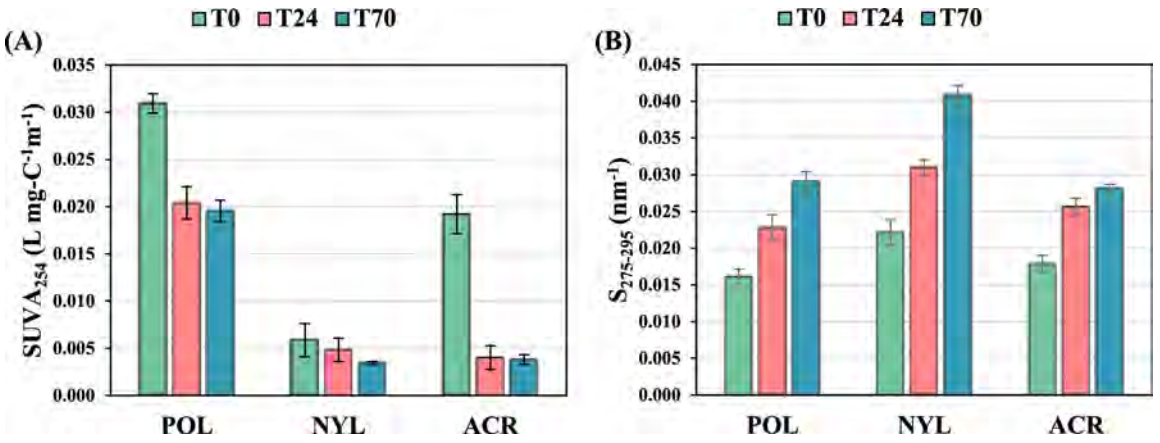

Figure 4. Variations in optical properties of DOM released from MFs (POL, NYL, and ACR): (a) specific UV absorbance at 254 nm ($SUVA_{254}$) and (b) spectral slope value between 275 and 295 nm ($S_{275-295}$).

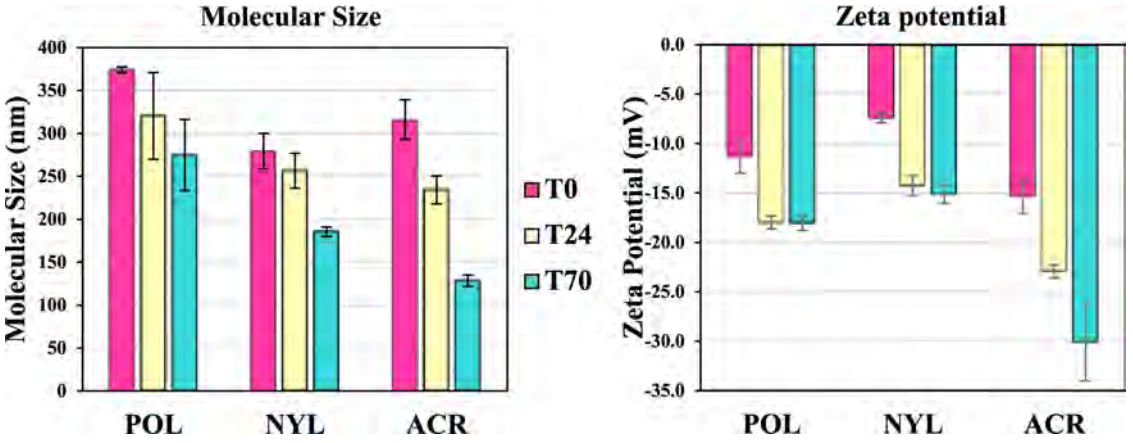

Figure 5. Molecular size and zeta potential of DOM released from MFs during UV irradiation as characterized using the dynamic light scattering technique (Zetasizer).

order production pattern (Figure 3). On the other hand, considerable UV-induced degradation and fragmentation were observed on the surfaces of both nylon and acrylic fibers, with chain scission and evident fiber damage (Figure 1), leading to an exponential release of DOM from both nylon and acrylic (Figure 3).

Specifically, concentrations of DOC increased significantly after 4 h of degradation for all pristine microfibers compared to their corresponding background DOC before UV irradiation or those in dark treatments ($p = 0.0005$ for POL-DOC, $p = 0.007$ for NYL-DOC, and $p = 0.006$ for ACR-DOC). Both NYL and ACR produced much higher DOM than POL during photochemical degradation, with DOC concentrations at 70 h approaching 13.32 and 10.63 mg/L, respectively, compared to 0.89 mg/L for POL (Figure 3). Distinctively, low DOC production from POL can be attributed to its hydrophobic properties, which repel water and lower DOM release.[61,62] Our result here is consistent with findings from a previous study on the chemical degradation of polyester material exposed to seawater for a year.[63] They observed a relative weight loss of about 7% and chemical restructuring of the polymer with a shift in carbonyl, ester, and vinyl groups.[63]

From a CDOM perspective, the DOM generated from MFs closely resembled the DOC pattern. Acrylics exhibited a CDOM production rate 3.4 times higher than that of POL and 1.7 times higher than that of NYL (Figure 3), consistent with their changes in surface morphology and Raman spectra under UV irradiation (see Figures 1 and 2).

3.3. Characterization of MF-Released DOM: $SUVA_{254}$ and Spectral Slope. Variations in optical properties, including $SUVA_{254}$ and $S_{275-295}$, of DOM released from MFs before and during their photochemical degradation are shown in Figure 4 and Figure S1 of the Supporting Information. While DOM released from POL was low in concentrations (Figure 3), it had higher aromaticity or $SUVA_{254}$ values compared to DOM released from other microfibers (Figure 4A). Higher $SUVA_{254}$ values observed for POL-DOM are consistent with the presence of unique aromatic structures or terephthalate groups in polyester but not in nylon, which contains polyamide, or in acrylic, which typically contains polyacrylonitrile (Table 1). It is interesting to note that, although DOM concentrations increased consistently during photochemical weathering of all microfibers, $SUVA_{254}$ values of DOM decreased slightly during DOM production from the degradation of MFs. The measurable decrease in $SUVA_{254}$ values suggested that, in addition to DOM production during MFs' weathering, portions of the MF-released DOM were concurrently degraded, especially the aromatic DOM components that contribute to a higher $SUVA_{254}$ value.[45] The preferential removal of aromatic chromophores and/or the breakdown of aromatic compounds evidently resulted in a decrease in $SUVA_{254}$ values.[36,47]

https://doi.org/10.1021/acs.est.4c03667
Environ. Sci. Technol. 2024, 58, 16535−16546

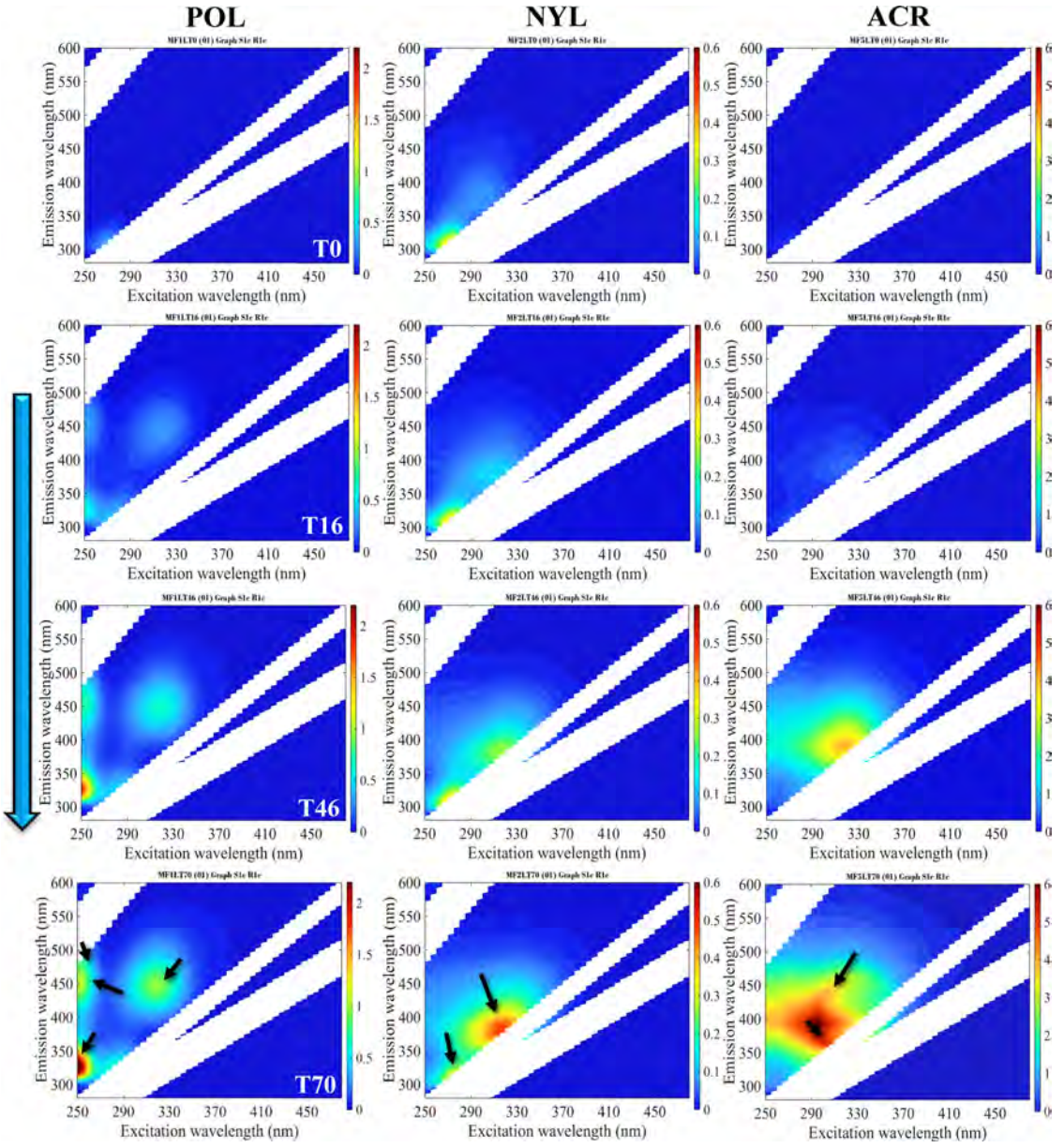

Figure 6. Fluorescence EEMs of MF-released DOM during photochemical weathering of MFs, including POL, NYL, and ACR, demonstrating a consistent increase in fluorescence intensities and a continuous release of DOM from MFs during their photochemical degradation at the starting point (T0), 16 h (T16), 46 h (T46), and 70 h (T70).

Spectral slope values ($S_{275-295}$) provide information on the molecular weight of DOM.[46] As depicted in Figure 4B, an increase in $S_{275-295}$ values was observed for DOM produced during the degradation of MFs, which corresponds to a decrease in the molecular weight of the DOM pool. The increase in $S_{275-295}$ values or decrease in apparent DOM molecular weight suggested that higher molecular weight DOM seemed to degrade or breakdown preferentially during UV irradiation, leading to a consequent reduction in the overall molecular weight and aromaticity of DOM.[36,64,66] These results coincide with those from the photodegradation of natural DOM[67,68] and water-soluble plastic-derived DOM.[36]

3.4. Surface Properties of MF-Derived DOM. Figure 5 illustrates variations in the molecular size and zeta potential of DOM released from MFs during UV irradiation. In general, the molecular size of MF-released DOM decreased during the photochemical degradation of MFs. For example, the molecular size of DOM decreased from ~310 to 275 nm for POL-DOM, from 280 to 180 nm for NYL-DOM, and from 260 to ~140 nm for ACR-DOM after degradation for 70 h (Figure 5). This decrease in molecular size indicated that UV irradiation indeed preferentially induces the degradation or breakdown of larger sized DOM. The findings obtained through dynamic light scattering (Figure 5) are consistent with those derived from spectral slope values, which exhibited an increase during the degradation of MFs (Figure 4). The changes in surface properties of DOM during DOM production from the photochemical weathering of MFs also suggest a simultaneous, selective, and small-scale DOM degradation, as illustrated in changes in optical properties, for both $SUVA_{254}$ and $S_{275-295}$ (Figure 4). Additionally, the observed molecular size ranges (140−310 nm) of the DOM released from MFs (Figure 5) suggest that the photo-weathering of MFs may lead to the production of nanofibers

https://doi.org/10.1021/acs.est.4c03667
Environ. Sci. Technol. 2024, 58, 16535−16546

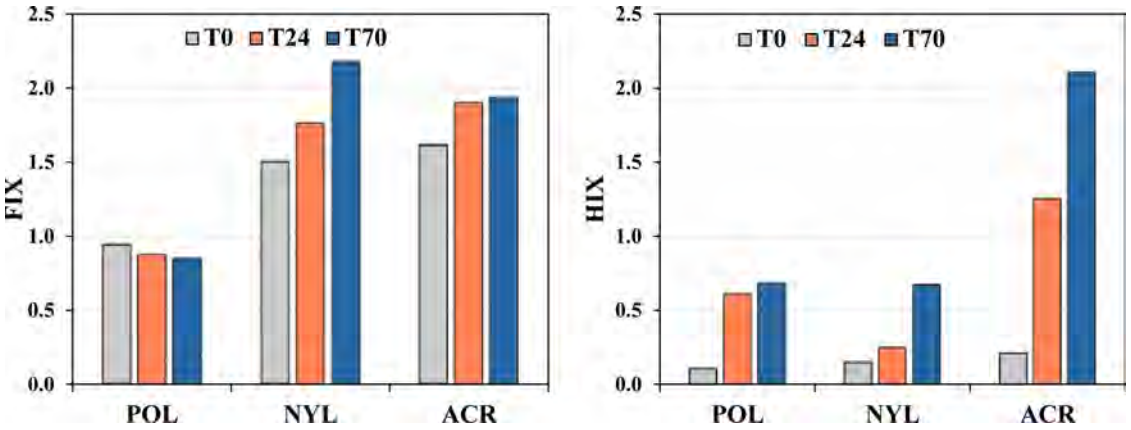

Figure 7. Variations of HIX and FIX in DOM released from MFs (POL, NYL, and ACR) during their photochemical degradation at the starting point (T0), 24 h (T24), and 70 h (T70).

or nanoplastics in aquatic environments, a phenomenon also suggested for other plastics in previous studies.[9,69,70] Further studies are needed to verify their polymeric structures in the MF-released DOM.

With regard to the zeta potential, all MF-derived DOM was negatively charged, with a zeta potential ranging from −7.5 mV for NYL-DOM to −15 mV for ACR-DOM (Figure 5). In comparison to the initial DOM, the zeta potential values of DOM collected at the end of UV irradiation (70 h) become more negative (∼−30 mV for ACR-DOM). The observed trend of increasingly negative zeta potential postdegradation is noteworthy. The more negative zeta potential indicates a higher repulsive force among DOM molecules, suggesting enhanced stability and reduced aggregation. This phenomenon is consistent with the formation of smaller nanofibers or nanoplastics during microfiber degradation, where the increased surface area exposes more charged sites, leading to a heightened negative zeta potential. For example, the regression analysis for ACR-DOM (R^2 = 0.99) reveals that approximately 99.19% of the variability in zeta potential over time can be accounted for by the size of ACR-DOM. The correlation coefficients (R^2 = 0.892, 0.758, and 0.996) indicate that size and zeta potential have a strong, moderate to significantly positive linear correlation in POL-DOM, NYL-DOM, and ACR-DOM, respectively.

The simultaneous decrease in both molecular size and zeta potential or the increase in absolute zeta potential values indicated that DOM molecules could become more stable or less prone to aggregate after being released from MFs during photochemical weathering. More importantly, the DOM released during photochemical weathering of MFs is nanofibers in nature with high specific surface areas and high negative charge. These colloidal characteristics have significant environmental implications in aquatic systems for the fate and transport of trace elements and emerging contaminants. Future studies are needed to evaluate the role of MF-released DOM in the environment.

3.5. Fluorescence Characterization of MF-Derived DOM. Fluorescence EEMs of MF-released DOM and their changes during DOM production under UV irradiation are depicted in Figure 6. Changes in the EEM spectra showed the emergence of fluorophore peaks and a consistent increase in their fluorescence intensities in DOM released during the photochemical degradation of MFs compared to those from the dark incubation of MFs (Figure S2 of the Supporting Information). These results for changes in fluorescence EEMs (Figure 6) are consistent with the patterns observed for both DOC and CDOM, as shown in Figure 3.

As evident from the EEM contours of POL-DOM, three fluorescent peaks become visible at T16, including peak A (ex/em = 260/400−460 nm) and peak C (ex/em = 320−360/420−460 nm), which are associated to humic-like fluorophores, and peak B (ex/em = 250/325 nm) and peak T (ex/em = 275/340 nm), which are related to protein-like fluorophores.[71,72] On the other hand, NYL-DOM had two different fluorescence peaks: one inherent was bleached during UV irradiation, and new fluorophores emerged in the region matching humic-like peak M at ex/em = 310/380 nm.[65,71] In addition, ACR-DOM exhibited three fluorescence peaks corresponding to humic-like fluorophores, including peak A (ex/em = 260/380−460 nm), peak M (ex/em = 290/350−410 nm), and peak C (ex/em = 320/420−460 nm).[65,71] The observed rise in fluorescence intensities of these fluorophore peaks originating from MF-derived DOM aligns closely with the impact of UV irradiation on fibers, as evidenced by SEM images as well as the trends in DOC and CDOM production discussed above.

Fluorescence indices, including both the humification index (HIX) and fluorescence index (FIX), were utilized to monitor changes in DOM characteristics during the production of DOM from MF degradation. As shown in Figure 7, both HIX and FIX increased significantly in DOM released from MFs under UV irradiation, except for POL-DOM, which showed a slight decrease in FIX values. Notably, the increase in the DOC and CDOM concentrations during the photochemical weathering of MFs was accompanied by the increase in HIX values (Figures 3 and 7). The positive correlations between HIX and the DOC or CDOM concentration attest to an elevated DOM production during the photochemical weathering of MFs.

3.6. DOM Production Kinetics during Photochemical Weathering of MFs. On the basis of the time-series data of both DOC and CDOM (Figure 3) and assuming a zero-order DOM production, we estimated the production rate constants (k, in milligrams per hour) of DOM under the same weight/volume ratio for all microfibers. The production rate constants or k values follow the order of ACR-DOM > NYL-DOM > POL-DOM, with the same trend for DOC and CDOM (Figure 8). This corresponds to a higher photochemical reactivity for ACR, followed by NYL and POL. However, the production rate constants for DOC were higher compared to

https://doi.org/10.1021/acs.est.4c03667
Environ. Sci. Technol. 2024, 58, 16535−16546

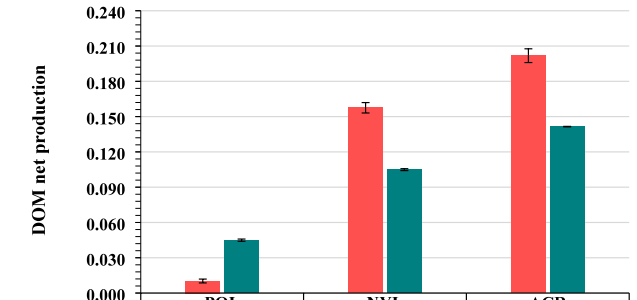

	POL	NYL	ACR
DOC (mg-C/h)	0.010	0.158	0.202
CDOM (AU/h)	0.045	0.105	0.141

Figure 8. Production rate constants of DOC (mg-C/h) and CDOM (AU/h) released from microfibers during photochemical weathering.

those of CDOM, except for NYL-DOM, consistent with the fact that CDOM comprises only a portion of bulk DOM.[43] In addition, POL had a lower DOM production rate constant, as manifested in the linear increase in both DOC and CDOM concentrations (Figure 3). This observation is supported by SEM images depicting the morphology of their corresponding fiber surfaces (Figure 1). In contrast, both NYL and ACR had higher DOM production rate constants, as also evidenced by the exponential increases in both DOC and CDOM levels during the photochemical degradation of the respective microfibers (Figure 3). Previous studies have shown that the UV degradation of MFs could be markedly enhanced under higher humidity conditions, suggesting a more pronounced degradation of polymers in surface waters than in dry environments.[73] Microscopic perforation has been identified on the surfaces of polycarbonate films following hydrolytic degradation and in fibers during degradation under natural conditions.[74,75]

The relationship between the degradation rates of MFs and their polymer structures is complex. For example, polyester, which contains both terephthalate and ester groups (Table 1), undergoes photodegradation primarily through hydrolysis and the cleavage of ester bonds[76] yet exhibits the lowest degradation rate among all three microfibers, despite its high aromaticity in the released DOM (Figures 3 and 8). The unique polyethylene terephthalate (PET)-containing backbone of polyester could absorb the UV light at the surface[77] and has a high propensity for cross-linking reactions,[78] potentially preventing further degradation of POL and leading to its relative slow DOM release (Figures 3 and 8). While the presence of aromatic rings in POL (Table 1) contributes to higher aromaticity in POL-DOM, it paradoxically results in lower DOM production rates compared to NYL and ARC, highlighting the intricate interplay between polymer composition and degradation behavior. Nylon 66, which contains amide groups, degrades under UV exposure through the cleavage of amide bonds.[79] As shown in Figures 4 and 8, NYL-DOM had a lower aromaticity and lower apparent molecular weight but higher DOM production rates compared to POL-DOM, likely resulting from the breakdown of the C−N bonds in the amide linkages and the formation of smaller oligomers and monomers.[80] Among the three microfibers, acrylic (typically polyacrylonitrile) had the highest DOM production rate during photochemical weathering, as evidenced by its highest CDOM and fluorophore intensities with higher FIX and HIX (Figures 3, 6, and 7), even though ACR-DOM had the lowest aromaticity (Figure 4). The presence of conjugated double bonds may facilitate the degradation of acrylic through the cleavage of nitrile groups and the polymer backbone.[81,82] Detailed characterization of monomers and oligomers in the MF-released DOM is needed to better quantify the relationship between the degradation rate of MFs, chemical and surface properties of released DOM, and the polymer structure of microfibers.

Overall, these observations lend support to the hypothesis that photochemical degradation and hydrolysis may be concurrent processes in the weathering of microfibers.[41] These processes contribute to DOM production with specific rate constants that are dependent upon the type of MF or polymer involved. Therefore, the production rate constant is a useful proxy for evaluating the photochemical reactivity, weathering kinetics, and production of DOM from MFs. Future studies are needed to investigate the ecological and environmental roles of MF-derived DOM and nanofibers in aquatic environments.

■ ASSOCIATED CONTENT

Supporting Information

The Supporting Information is available free of charge at https://pubs.acs.org/doi/10.1021/acs.est.4c03667.

Comparisons in the normalized Raman peaks between pristine and weathered microfibers (Table S1), variations in DOC, CDOM, and specific UV absorbance at 254 nm ($SUVA_{254}$) of water-soluble DOM of MFs during pre-cleaning/washing before their photochemical degradation (Figure S1), and variations in fluorescence EEM spectra of MF-released DOM during dark incubation of microfibers, including POL, NYL, and ACR, at 0, 16, 46, and 70 h (Figure S2) (PDF)

■ AUTHOR INFORMATION

Corresponding Author

Laodong Guo − *School of Freshwater Sciences, University of Wisconsin—Milwaukee, Milwaukee, Wisconsin 53204, United States;* orcid.org/0000-0002-5010-1630; Phone: 414-382-1742; Email: guol@uwm.edu

Author

Shimaa M. Kteeba − *School of Freshwater Sciences, University of Wisconsin—Milwaukee, Milwaukee, Wisconsin 53204, United States; Faculty of Science, Damietta University, New Damietta, Damietta 34511, Egypt*

Complete contact information is available at: https://pubs.acs.org/10.1021/acs.est.4c03667

Author Contributions

Shimaa M. Kteeba performed the experiments, analyzed samples, and wrote the first version of the manuscript. Laodong Guo conceived the research, provided funding and supervision, and co-wrote the manuscript.

Notes

The authors declare no competing financial interest.

■ ACKNOWLEDGMENTS

The authors are grateful for the technical assistance from Dr. Hamed Sadabadi and Dr. Steven Hardcastle for the characterization of microfibers using SEM and Raman spectroscopy. The authors extend their gratitude to Tom Klaas, Testfabrics, Inc., for providing the microfiber samples, Dr. Fernando

Rosario-Ortiz, the executive editor, and three anonymous reviewers for their constructive comments, which greatly improved the manuscript. This work was supported in part by the National Science Foundation (NSF Award 2204145), the Freshwater Collaborative of Wisconsin (UWSA.09 and SL3.27), and the Discovery and Innovation Grant Program from University of Wisconsin—Milwaukee (DIG-101X405 and DIG-101X439). Shimaa M. Kteeba acknowledges support from the Egyptian Government Scholarship, The Cultural Affairs and Mission Sectors of the Egyptian Ministry of Higher Education.

REFERENCES

(1) Lim, X. Microplastics are everywhere—But are they harmful? *Nature* **2021**, *593*, 22−25.
(2) Stubbins, A.; Law, K. L.; Muñoz, S. E.; Bianchi, T. S.; Zhu, L. Plastics in the Earth system. *Science* **2021**, *373*, 51−55.
(3) Nizzetto, L.; Futter, M.; Langaas, S. Are Agricultural Soils Dumps for Microplastics of Urban Origin? *Environ. Sci. Technol.* **2016**, *50*, 10777−10779.
(4) Alimi, O. S.; Farner Budarz, J.; Hernandez, L. M.; Tufenkji, N. Microplastics and Nanoplastics in Aquatic Environments: Aggregation, Deposition, and Enhanced Contaminant Transport. *Environ. Sci. Technol.* **2018**, *52* (4), 1704−1724.
(5) Romera-Castillo, C.; Pinto, M.; Langer, T. M.; Álvarez-Salgado, X. A.; Herndl, G. J. Dissolved organic carbon leaching from plastics stimulates microbial activity in the ocean. *Nat. Commun.* **2018**, *9*, 1430.
(6) Zhu, L.; Zhao, S.; Bittar, T. B.; Stubbins, A.; Li, D. Photochemical dissolution of buoyant microplastics to dissolved organic carbon: Rates and microbial impacts. *J. Hazard. Mater.* **2020**, *383*, 121065.
(7) Yan, C.; Wang, X.; Nie, M.; Mo, X.; Ding, M.; Chen, J.; Yang, Y. Characteristics of microplastic-derived dissolved organic matter and its binding with pharmaceuticals unveiled by fluorescence spectroscopy and two-dimensional correlation spectroscopy. *Sci. Total Environ.* **2024**, *908*, 168190.
(8) Li, Y.; Lu, Q.; Xing, Y.; Liu, K.; Ling, W.; Yang, J.; Yang, Q.; Wu, T.; Zhang, J.; Pei, Z.; Gao, Z.; Li, X.; Yang, F.; Ma, H.; Liu, K.; Zhao, D. Review of research on migration, distribution, biological effects, and analytical methods of microfibers in the environment. *Sci. Total Environ.* **2023**, *855*, 158922.
(9) Lambert, S.; Wagner, M. Characterisation of nanoplastics during the degradation of polystyrene. *Chemosphere* **2016**, *145*, 265−268.
(10) Hernandez, L. M.; Grant, J.; Fard, P. S.; Farner, J. M.; Tufenkji, N. Analysis of ultraviolet and thermal degradations of four common microplastics and evidence of nanoparticle release. *J. Hazard. Mat. Lett.* **2023**, *4*, 100078.
(11) Agbenyega, J. A Raman study of order in some complex polyesters. Ph.D. Dissertation, University of Southampton, Southampton, U.K., 1992.
(12) Cárdenas-Alcaide, M. F.; Godínez-Alemán, J. A.; González-González, R. B.; Iqbal, H. M.; Parra-Saldívar, R. Environmental impact and mitigation of micro (nano) plastics pollution using green catalytic tools and green analytical methods. *Green Anal. Chem.* **2022**, *3*, 100031.
(13) Lee, Y. K.; Hong, S.; Hur, J. Copper-binding properties of microplastic-derived dissolved organic matter revealed by fluorescence spectroscopy and two-dimensional correlation spectroscopy. *Wat. Res.* **2021**, *190*, 116775.
(14) Chen, M.; Xu, J.; Tang, R.; Yuan, S.; Min, Y.; Xu, Q.; Shi, P. Roles of microplastic-derived dissolved organic matter on the photodegradation of organic micropollutants. *J. Hazard. Mater.* **2022**, *440*, 129784.
(15) Mishra, S.; Rath, C. C.; Das, A. P. Marine microfiber pollution: A review on present status and future challenges. *Mar. Pollut. Bull.* **2019**, *140*, 188−197.
(16) Avio, C. G.; Pittura, L.; d'Errico, G.; Abel, S.; Amorello, S.; Marino, G.; Gorbi, S.; Regoli, F. Distribution and characterization of microplastic particles and textile microfibers in Adriatic food webs: General insights for biomonitoring strategies. *Environ. Pollut.* **2020**, *258*, 113766.
(17) Alvim, C. B.; Bes-Piá, M. A.; Mendoza-Roca, J. A.; Alonso-Molina, J. L. Identification of microfibers in drinking water with Nile Red. Limitations and strengths. *J. Environ. Chem. Eng.* **2023**, *11*, 109697.
(18) Suaria, G.; Achtypi, A.; Perold, V.; Lee, J. R.; Pierucci, A.; Bornman, T. G.; Aliani, S.; Ryan, P. G. Microfibers in oceanic surface waters: A global characterization. *Sci. Adv.* **2020**, *6* (23), No. eaay8493.
(19) Stanton, T.; Johnson, M.; Nathanail, P.; MacNaughtan, W.; Gomes, R. L. Freshwater and airborne textile fibre populations are dominated by 'natural', not microplastic, fibres. *Sci. Total Environ.* **2019**, *666*, 377−389.
(20) Finnegan, A. M. D.; Süsserott, R.; Gabbott, S. E.; Gouramanis, C. Man-made natural and regenerated cellulosic fibres greatly outnumber microplastic fibres in the atmosphere. *Environ. Pollut.* **2022**, *310*, 119808.
(21) Napper, I.; Parker-Jurd, F.; Wright, S.; Thompson, R. Examining the release of synthetic microfibres to the environment via two major pathways: Atmospheric deposition and treated wastewater effluent. *Sci. Total Environ.* **2023**, *857*, 159317.
(22) De Falco, F.; Cocca, M.; Avella, M.; Thompson, R. C. Microfiber release to water, via laundering, and to air, via everyday use: A comparison between polyester clothing with differing textile parameters. *Environ. Sci. Technol.* **2020**, *54* (6), 3288−3296.
(23) Deng, H.; Wei, R.; Luo, W.; Hu, L.; Li, B.; Di, Y. n.; Shi, H. Microplastic pollution in water and sediment in a textile industrial area. *Environ. Pollut.* **2020**, *258*, 113658.
(24) Duis, K.; Coors, A. Microplastics in the aquatic and terrestrial environment: Sources (with a specific focus on personal care products), fate and effects. *Environ. Sci. Europe* **2016**, *28*, 1−25.
(25) Boucher, J.; Friot, D. *Primary Microplastics in the Oceans: A Global Evaluation of Sources*; International Union for Conservation of Nature (IUCN): Gland, Switzerland, 2017; DOI: 10.2305/IUCN.-CH.2017.01.en.
(26) Sun, J.; Dai, X.; Wang, Q.; van Loosdrecht, M. C. M.; Ni, B.-J. Microplastics in wastewater treatment plants: Detection, occurrence and removal. *Water Res.* **2019**, *152*, 21−37.
(27) Chatterjee, N. H.; Manna, S.; Ray, A.; Das, S.; Rana, N.; Banerjee, A.; Ray, M.; Ray, S. Microplastics contamination in two species of gobies and their estuarine habitat of Indian Sundarbans. *Mar. Pollut. Bull.* **2024**, *198*, 115857.
(28) Gago, J.; Carretero, O.; Filgueiras, A. V.; Viñas, L. Synthetic microfibers in the marine environment: A review on their occurrence in seawater and sediments. *Mar. Pollut. Bull.* **2018**, *127*, 365−376.
(29) Sanchez-Vidal, A.; Thompson, R. C.; Canals, M.; de Haan, W. P. The imprint of microfibres in southern European deep seas. *PLoS One* **2018**, *13*, No. e0207033.
(30) Woods, M. N.; Stack, M. E.; Fields, D. M.; Shaw, S. D.; Matrai, P. A. Microplastic fiber uptake, ingestion, and egestion rates in the blue mussel (Mytilus edulis). *Mar. Pollut. Bull.* **2018**, *137*, 638−645.
(31) Kutralam-Muniasamy, G.; Pérez-Guevara, F.; Elizalde-Martínez, I.; Shruti, V. C. An overview of recent advances in micro/nano beads and microfibers research: Critical assessment and promoting the less known. *Sci. Total Environ.* **2020**, *740*, 139991.
(32) Singh, R. P.; Mishra, S.; Das, A. P. Synthetic microfibers: Pollution toxicity and remediation. *Chemosphere* **2020**, *257*, 127199.
(33) Bhagwat, G.; Tran, T. K. A.; Lamb, D.; Senathirajah, K.; Grainge, I.; O'Connor, W.; Juhasz, A.; Palanisami, T. Biofilms Enhance the Adsorption of Toxic Contaminants on Plastic Microfibers under Environmentally Relevant Conditions. *Environ. Sci. Technol.* **2021**, *55*, 8877−8887.
(34) Sharma, M. D.; Krupadam, R. J. Adsorption-desorption dynamics of synthetic and naturally weathered microfibers with toxic heavy metals and their ecological risk in an estuarine ecosystem. *Environ. Res.* **2022**, *207*, 112198.

(35) Yang, T.; Xu, Y.; Liu, G.; Nowack, B. Oligomers are a major fraction of the released submicrometre particles released during washing of polyester textiles. *Nat. Water* **2024**, *2*, 151−160.
(36) Schutte, M. M.; Kteeba, S. M.; Guo, L. Photochemical reactivity of water-soluble dissolved organic matter from microplastics and microfibers. *Sci. Total Environ.* **2024**, *911*, 168616.
(37) Lee, Y. K.; Murphy, K. R.; Hur, J. Fluorescence Signatures of Dissolved Organic Matter Leached from Microplastics: Polymers and Additives. *Environ. Sci. Technol.* **2020**, *54*, 11905−11914.
(38) Liu, J.; Liu, Q.; An, L.; Wang, M.; Yang, Q.; Zhu, B.; Ding, J.; Ye, C.; Xu, Y. Microfiber Pollution in the Earth System. *Rev. Environ. Contam. Toxicol.* **2022**, *260* (1), 1−16.
(39) Rodríguez-Narvaez, O. M.; Goonetilleke, A.; Perez, L.; Bandala, E. R. Engineered technologies for the separation and degradation of microplastics in water: A review. *Chem. Eng. J.* **2021**, *414*, 128692.
(40) Sutkar, P. R.; Gadewar, R. D.; Dhulap, V. P. Recent trends in degradation of microplastics in the environment: A state-of-the-art review. *J. Hazard. Mat. Adv.* **2023**, *11*, 100343.
(41) Sørensen, L.; Groven, A. S.; Hovsbakken, I. A.; Del Puerto, O.; Krause, D. F.; Sarno, A.; Booth, A. M. UV degradation of natural and synthetic microfibers causes fragmentation and release of polymer degradation products and chemical additives. *Sci. Total Environ.* **2021**, *755*, 143170.
(42) Guo, L.; Santschi, P. H. Measurements of dissolved organic carbon (DOC) in sea water by high temperature combustion method. *Acta Oceanol. Sin.* **1997**, *16* (3), 339−353.
(43) Zhou, Z.; Guo, L.; Minor, E. C. Characterization of bulk and chromophoric dissolved organic matter in the Laurentian Great Lakes during summer 2013. *J. Great Lakes Res.* **2016**, *42*, 789−801.
(44) Lin, H.; Guo, L. Variations in Colloidal DOM Composition with Molecular Weight within Individual Water Samples as Characterized by Flow Field-Flow Fractionation and EEM-PARAFAC Analysis. *Environ. Sci. Technol.* **2020**, *54*, 1657−1667.
(45) Weishaar, J. L.; Aiken, G. R.; Bergamaschi, B. A.; Fram, M. S.; Fujii, R.; Mopper, K. Evaluation of Specific Ultraviolet Absorbance as an Indicator of the Chemical Composition and Reactivity of Dissolved Organic Carbon. *Environ. Sci. Technol.* **2003**, *37* (20), 4702−4708.
(46) Helms, J. R.; Stubbins, A.; Ritchie, J. D.; Minor, E. C.; Kieber, D. J.; Mopper, K. Absorption spectral slopes and slope ratios as indicators of molecular weight, source, and photobleaching of chromophoric dissolved organic matter. *Limnol. Oceanogr.* **2008**, *53* (3), 955−969.
(47) Du, Y.; Zhang, Y.; Chen, F.; Chang, Y.; Liu, Z. Photochemical reactivities of dissolved organic matter (DOM) in a sub-alpine lake revealed by EEM-PARAFAC: An insight into the fate of allochthonous DOM in alpine lakes affected by climate change. *Sci. Total Environ.* **2016**, *568*, 216−225.
(48) McKnight, D. M.; Boyer, E. W.; Westerhoff, P. K.; Doran, P. T.; Kulbe, T.; Andersen, D. T. Spectrofluorometric characterization of dissolved organic matter for indication of precursor organic material and aromaticity. *Limnol. Oceanogr.* **2001**, *46*, 38−48.
(49) Ohno, T. Fluorescence Inner-Filtering Correction for Determining the Humification Index of Dissolved Organic Matter. *Environ. Sci. Technol.* **2002**, *36*, 742−746.
(50) Kteeba, S. M.; El-Adawi, H. I.; El-Rayis, O. A.; El-Ghobashy, A. E.; Schuld, J. L.; Svoboda, K. R.; Guo, L. Zinc oxide nanoparticle toxicity in embryonic zebrafish: Mitigation with different natural organic matter. *Environ. Pollut.* **2017**, *230*, 1125−1140.
(51) Sørensen, L.; Rogers, E.; Altin, D.; Salaberria, I.; Booth, A. M. Sorption of PAHs to microplastic and their bioavailability and toxicity to marine copepods under co-exposure conditions. *Environ. Pollut.* **2020**, *258*, 113844.
(52) Nava, V.; Frezzotti, M. L.; Leoni, B. Raman Spectroscopy for the Analysis of Microplastics in Aquatic Systems. *Appl. Spectrosc.* **2021**, *75*, 1341−1357.
(53) McGraw, G. E. Investigation of Polyester Structure by Laser Raman Spectroscopy. In *Polymer Characterization Interdisciplinary Approaches*; Craver, C. D., Ed.; Springer: Boston, MA, 1971, pp 37−46, DOI: 10.1007/978-1-4684-1929-0_3.
(54) Puchowicz, D.; Cieslak, M. Raman spectroscopy in the analysis of textile structures. In *Recent Developments in Atomic Force Microscopy and Raman Spectroscopy for Materials Characterization*; Shakher Pathak, C., Kumar, S., Eds.; IntechOpen: London, U.K., 2022; Chapter 9, pp 1−21, DOI: 10.5772/intechopen.99731.
(55) Bodnaryk, W. J.; Li, K.; Adronov, A. UV-light mediated decomposition of a polyester for enrichment and release of semiconducting carbon nanotubes. *J. Polym. Sci.* **2020**, *58* (14), 1965−1972.
(56) Halim, S. F.; Abou-Kandil, A. I.; Awad, A.; Darwish, N. In situ Grafting of Maleic Anhydride Onto Natural Rubber to Improve Its Adhesion to Polyester Fabric: Mechanical and Spectroscopic Analyses. *J. Adhes. Sci. Technol.* **2009**, *23* (1), 71−83.
(57) Nishikida, K.; Coates, J. Infrared and Raman Analysis of Polymers. In *Handbook of Plastics Analysis*; Lobo, H., Bonilla, J., Eds.; CRC Press: Boca Raton, FL, 2003; Chapter 7, pp 189−328, DOI: 10.1201/9780203911983.ch7.
(58) Stephens, J. S.; Chase, D. B.; Rabolt, J. F. Effect of the Electrospinning Process on Polymer Crystallization Chain Conformation in Nylon-6 and Nylon-12. *Macromolecules* **2004**, *37*, 877−881.
(59) Miller, J. V.; Bartick, E. G. Forensic analysis of single fibers by Raman spectroscopy. *Appl. Spectrosc.* **2001**, *55*, 1729−1732.
(60) Lee, E.; O'Donnell, B. Characterizing Microplastic Fibers Using Raman Spectroscopy. *Spectrosc. Suppl.* **2019**, *34*, 32−40.
(61) Azeem, M.; Javed, A.; Morikawa, H.; Noman, M. T.; Khan, M. Q.; Shahid, M.; Wiener, J. Hydrophilization of polyester textiles by nonthermal plasma. *Autex Res. J.* **2021**, *21* (2), 142−149.
(62) Lee, D. W.; Little, T. J. Difference in hydrophobic and hydrophilic multilayered systems. *Measurement* **2013**, *46* (2), 920−927.
(63) Muthukumar, T.; Aravinthan, A.; Lakshmi, K.; Venkatesan, R.; Vedaprakash, L.; Doble, M. Fouling and stability of polymers and composites in marine environment. *Int. Biodeter. Biodegr.* **2011**, *65* (2), 276−284.
(64) Paul, A.; Dziallas, C.; Zwirnmann, E.; Gjessing, E. T.; Grossart, H.-P. UV irradiation of natural organic matter (NOM): Impact on organic carbon and bacteria. *Aquatic Sci.* **2012**, *74*, 443−454.
(65) Coble, P. G. Characterization of marine and terrestrial DOM in seawater using excitation-emission matrix spectroscopy. *Mar. Chem.* **1996**, *51* (4), 325−346.
(66) Ateia, M.; Apul, O. G.; Shimizu, Y.; Muflihah, A.; Yoshimura, C.; Karanfil, T. Elucidating Adsorptive Fractions of Natural Organic Matter on Carbon Nanotubes. *Environ. Sci. Technol.* **2017**, *51* (12), 7101−7110.
(67) Chari, N. V. H. K.; Keerthi, S.; Sarma, N. S.; Pandi, S. R.; Chiranjeevulu, G.; Kiran, R.; Koduru, U. Fluorescence and absorption characteristics of dissolved organic matter excreted by phytoplankton species of western Bay of Bengal under axenic laboratory condition. *J. Exp. Mar. Biol. Ecol.* **2013**, *445*, 148−155.
(68) Xu, H.; Guan, D.-X.; Zou, L.; Lin, H.; Guo, L. Contrasting effects of photochemical and microbial degradation on Cu(II) binding with fluorescent DOM from different origins. *Environ. Pollut.* **2018**, *239*, 205−214.
(69) Pathan, S. I.; Arfaioli, P.; Bardelli, T.; Ceccherini, M. T.; Nannipieri, P.; Pietramellara, G. Soil Pollution from Micro- and Nanoplastic Debris: A Hidden and Unknown Biohazard. *Sustainability* **2020**, *12* (18), 7255.
(70) Bai, X.; Li, F.; Ma, L.; Li, C. Weathering of geotextiles under ultraviolet exposure: A neglected source of microfibers from coastal reclamation. *Sci. Total Environ.* **2022**, *804*, 150168.
(71) Coble, P. G. Marine Optical Biogeochemistry: The Chemistry of Ocean Color. *Chem. Rev.* **2007**, *107* (2), 402−418.
(72) Murphy, K. R.; Butler, K. D.; Spencer, R. G.; Stedmon, C. A.; Boehme, J. R.; Aiken, G. R. Measurement of dissolved organic matter fluorescence in aquatic environments: An interlaboratory comparison. *Environ. Sci. Technol.* **2010**, *44* (24), 9405−9412.

(73) Lock, L. M.; Frank, G. C. A study of some factors affecting the Photodegradation of textile yarns part II: Nylon 66 and polyethylene terephthalate yarns. *Textile Res. J.* **1973**, *43*, 502−512.
(74) Chandure, A. S.; Bhusari, G. S.; Umare, S. S. Synthesis, characterization, and biodegradation studies of poly(1,4-cyclohexanedimethylene-adipate-carbonate)s. *J. Polym.* **2014**, *2014* (10), 1−11.
(75) Sathish, N.; Jeyasanta, K. I.; Patterson, J. Abundance, characteristics and surface degradation features of microplastics in beach sediments of five coastal areas in Tamil Nadu, India. *Mar. Pollut. Bull.* **2019**, *142*, 112−118.
(76) Gewert, B.; Plassmann, M. M.; MacLeod, M. Pathways for degradation of plastic polymers floating in the marine environment. *Environ. Sci.-Proc. Imp.* **2015**, *17* (9), 1513−1521.
(77) Hebner, T. S.; Maurer-Jones, M. A. Characterizing Microplastic Size and Morphology of Photodegraded Polymers Placed in Simulated Moving Water Conditions. *Environ. Sci.: Processes Impacts* **2020**, *22* (2), 398−407.
(78) Maurer-Jones, M. A.; Monzo, E. M. Quantifying Photochemical Transformations of Poly (butylene adipate-co-terephthalate) Films. *ACS Appl. Polym. Mater.* **2021**, *3* (2), 1003−1011.
(79) Thanki, P. N.; Singh, R. P. Photo-Oxidative Degradation of Nylon 66 under Accelerated Weathering. *Polymer* **1998**, *39* (25), 6363−6367.
(80) Do, C. H.; Pearce, E. M.; Bulkin, B. J.; Reimschuessel, H. K. FT-IR Spectroscopic Study on the Photo- and Photooxidative Degradation of Nylons. *J. Polym. Sci., Part A: Polym. Chem.* **1987**, *25* (8), 2301−2321.
(81) Guillet, J. E. *Polymers and Light*; Springer-Verlag: Berlin, Germany, 1985.
(82) Kaczmarek, H.; Chaberska, H.; Kowalonek, J. UV Light Induced Changes in Polyacrylonitrile. *Polymer* **2001**, *42* (19), 8385−8392.

https://doi.org/10.1021/acs.est.4c03667
Environ. Sci. Technol. 2024, 58, 16535−16546